Atmos. Chem. Phys., 26, 16939–16956, 2026
https://doi.org/10.5194/acp-26-16939-2026
© Author(s) 2026. This work is distributed under
the Creative Commons Attribution 4.0 License.

Atmospheric Chemistry and Physics
Open Access
EGU

Enhanced cirrus response to upper-tropospheric Saharan dust over Central Europe: evidence from Hungary (2001–2025)

György Varga[1,2], **Fruzsina Gresina**[1], **András Gelencsér**[2,3], **Adrienn Csávics**[1], **and Ágnes Rostási**[2,3]

[1]HUN-REN Research Centre for Astronomy and Earth Sciences, Budapest, Hungary
[2]Research Institute of Biomolecular and Chemical Engineering, University of Pannonia, Veszprém, Hungary
[3]MTA-PE Air Chemistry Research Group, Research Institute of Biomolecular and Chemical Engineering, University of Pannonia, Veszprém, Hungary

Correspondence: György Varga (varga.gyorgy@csfk.org)

Received: 25 June 2026 – Discussion started: 10 July 2026
Revised: 5 November 2026 – Accepted: 16 November 2026 – Published: 25 November 2026

Abstract. Saharan mineral dust is an important source of ice-nucleating particles, yet the long-term evolution of its relationship with upper-tropospheric ice clouds remains poorly constrained. Here, we investigate dust–cloud interactions over Hungary during 2001–2025 using MERRA-2, MODIS, and HIRS data, focusing on 276 independently identified Saharan dust events (SDEs). Vertically resolved MERRA-2 dust fields were used to quantify mineral dust at 7–12 km, allowing cloud properties to be compared between SDEs with different upper-tropospheric dust abundances and low-dust reference conditions. SDEs with high Dust7–12 were characterized by enhanced cirrus reflectance and high-cloud fraction and by higher, colder cloud tops in all seasons. The response was particularly coherent in spring, when cirrus reflectance and high-cloud fraction were 272 % and 133 % higher, respectively, effective ice particle radius was 7.2 % smaller, and outgoing longwave radiation was 14.4 % lower than under low-dust conditions. Springtime five-year composites showed no monotonic increase in Dust7–12, whereas the cirrus-reflectance enhancement increased from 143 % in 2001–2005 to 398 % in 2021–2025. These results indicate an increasingly pronounced springtime cirrus optical response during SDEs containing substantial dust at cirrus-relevant altitudes, while other cloud properties exhibit more variable long-term behaviour.

1 Introduction

Cirrus clouds represent one of the most important cloud types in the upper troposphere and play a key role in the Earth's radiation budget and climate feedback processes (Liou, 1986; Lolli et al., 2026; Storelvmo, 2017; Twomey, 1974). Located at high altitudes and composed predominantly of ice crystals, cirrus clouds are capable of both partially reflecting incoming shortwave solar radiation and absorbing and re-emitting outgoing longwave radiation from the Earth's surface (Boucher et al., 2013). Due to their low emission temperatures, cirrus clouds generally exert a positive radiative forcing, particularly when they are optically thin. Consequently, changes in cirrus cloud occurrence and upper-tropospheric humidity conditions have become a major focus of climate research.

Their radiative effect depends strongly on cloud altitude, optical thickness, ice crystal concentration, particle size and habit, and may therefore range from shortwave cooling to pronounced longwave warming (Heymsfield et al., 2017; Liou, 1986). Cirrus clouds also encompass a wide variety of formation pathways and microphysical states, ranging from in situ cirrus formed directly at low upper-tropospheric temperatures to liquid-origin cirrus developing from the glaciation of pre-existing mixed-phase clouds (Krämer et al., 2016, 2020; Krämer et al., 2025). Their formation is critically controlled by temperature, ice supersaturation, vertical motion, and the availability and ice-nucleating ability of aerosol par-

ticles. Consequently, relatively small changes in the thermodynamic environment or aerosol population may alter ice crystal number concentrations and cloud optical properties, with potential consequences for cirrus persistence and radiative effects (Kanji et al., 2017; Knopf and Alpert, 2023).

A central challenge in representing cirrus clouds in atmospheric models is the competition between homogeneous freezing and heterogeneous ice nucleation. Homogeneous freezing of solution droplets generally requires high ice supersaturation and can produce large numbers of ice crystals, whereas heterogeneous nucleation on ice-nucleating particles (INPs) can initiate ice formation at lower supersaturation and modify the subsequent evolution of the cloud (Kärcher et al., 2022, 2023).

In recent years, changes in upper-tropospheric cirrus conditions and ice-supersaturated regions (ISSRs) have attracted increasing scientific attention from a wide range of atmospheric observation and modelling studies (Benetatos et al., 2024). Observed changes in the Earth's radiation budget, the formation of extensive cirrus shields that can substantially reduce surface solar irradiance, and the climatic effects of persistent aircraft contrails and contrail-induced cirrus have all highlighted the importance of understanding upper-tropospheric cloud processes (Irvine and Shine, 2015; Kärcher, 2018).

The geographical distribution of increasing ISSR occurrence exhibits considerable spatial variability. Particularly pronounced changes have been observed over the Northern Hemisphere mid-latitudes, including Europe and the North Atlantic region, where increases in ISSR frequency ($+0.2\,\%$ to $+1.2\,\%$ per decade) substantially exceed the global average. These short-lived yet microphysically critical atmospheric states provide favourable thermodynamic conditions for ice crystal formation. Mineral dust is particularly relevant in this context because it represents one of the most important atmospheric sources of INPs, although its activity depends strongly on particle concentration, mineralogical composition, temperature, and nucleation mode (DeMott et al., 2003, 2010; Niemand et al., 2012; Ullrich, 2017). Model simulations therefore indicate that the response of cirrus clouds to mineral dust is not necessarily monotonic: enhanced heterogeneous nucleation may modify or suppress subsequent homogeneous freezing, while variations in vertical velocity and supersaturation can substantially change the resulting ice crystal population (Kärcher et al., 2022, 2023). Assessing dust–cirrus interactions thus requires consideration not only of atmospheric dust loading, but also of whether mineral dust reaches cirrus-forming altitudes and encounters thermodynamic and dynamical conditions favourable for heterogeneous ice nucleation.

In this context, Saharan mineral dust plays a particularly important role (Ansmann et al., 2019; Seifert et al., 2023; Weger et al., 2018). During long-range transport events, large quantities of mineral dust can reach Europe, including Central Europe (Ansmann et al., 2003; Pey et al., 2013; Rogora et al., 2004; Salvador et al., 2022; Varga, 2020). Mineral aerosol particles, especially those rich in K-feldspar, quartz and calcite, are known to act as highly efficient heterogeneous ice nuclei under the low-temperature conditions of the upper troposphere (Atkinson et al., 2013; Chatziparaschos et al., 2023; Harrison et al., 2019; Hoose et al., 2008; Hoose and Möhler, 2012; Seifert et al., 2010). The presence of mineral dust can promote heterogeneous ice nucleation at much lower ice supersaturation than required for homogeneous freezing and may thereby significantly modify ice crystal populations and the optical and radiative properties of cirrus clouds (Kok et al., 2023; Storelvmo, 2017).

Increasing trends in the frequency of Saharan dust intrusion events have been identified across Europe, including Central Europe, with the strongest increases occurring during approximately the last two decades. (Cuevas-Agulló et al., 2024; Rodríguez and López-Darias, 2024; Salvador et al., 2022; Varga, 2020). According to regional dust climatologies, Saharan dust-laden air masses have reached Central Europe on average 8–12 times per year in recent years (Varga, 2020). The most pronounced reductions in solar irradiance have been observed during spring and autumn dust events, when indirect radiative effects associated with cloud modification were found to play a dominant role (Varga et al., 2026). Previous studies have linked these changes to increasingly meridional atmospheric circulation patterns and a more meandering jet stream, which facilitate long-range dust transport while simultaneously influencing a wide range of hydrological and thermodynamic processes (Varga, 2020). Through their impacts on multiple climate zones, these circulation changes may exert complex influences on cloud formation and persistence.

Despite these large-scale atmospheric changes, previous investigations have demonstrated that the contribution of Saharan dust to cirrus formation and the associated reduction in surface irradiance can be clearly identified and quantified (Varga et al., 2026). Enhanced cloud reflectance, increased optical thickness, and greater cloud persistence have been observed during dust intrusion events, indicating a substantial influence of mineral dust on cirrus cloud development (Varga et al., 2026) (Fig. 1). Figure 1 illustrates several examples of extensive upper-level cloud shields occurring in association with Saharan dust transport over Europe. The spatial organization of these cloud systems resembles the dust-infused baroclinic storm (DIBS) structures described by Ansmann et al. (2019), in which mineral dust is transported into the upper troposphere within dynamically active weather systems. Such situations provide a physically plausible environment for dust–cirrus interactions, particularly when ascending air masses transport mineral particles into ice-supersaturated layers. Nevertheless, the satellite imagery alone does not establish the vertical overlap between dust and cirrus or demonstrate dust-induced ice nucleation. Nevertheless, long-term studies investigating regional trends in dust-associated cirrus changes remain scarce in Central Eu-

rope. In particular, there is still limited understanding of the processes linking increasing Saharan dust activity, changing upper-tropospheric moisture conditions, and long-term modifications of cirrus cloud properties (Ansmann et al., 2019; Seifert et al., 2023; Weger et al., 2018).

The aim of this study is to investigate the long-term relationship between Saharan mineral dust and upper-level ice-cloud properties over Hungary during 2001–2025, with particular emphasis on whether these associations have changed over time. By combining event-based, total-column, and vertically resolved dust metrics with satellite-derived cloud and radiative properties, we further assess whether dust reaching cirrus-relevant altitudes provides additional evidence for physically plausible dust–cirrus interactions within a changing atmospheric background.

A further objective is to examine the extent to which the observed cirrus cloud changes may be linked to evolving upper-tropospheric moisture conditions and the increasing occurrence of ice-saturated and ice-supersaturated environments. Although the study does not directly investigate ISSR climatology, the observed dust–cirrus relationships are interpreted within the broader context of ongoing thermodynamic changes in the upper troposphere.

2 Methods

2.1 Study area

The study focuses on Hungary, located in the Carpathian Basin, Central Europe (all of the analyses were conducted using the shapefile defining the national borders). Due to its geographical location, the region is situated at the intersection of several major atmospheric circulation systems, where Atlantic, Mediterranean, and continental influences all play important roles. The region is particularly sensitive to Saharan dust intrusions, which occur most frequently and intensely during the spring and summer seasons (Varga, 2020).

2.2 Dust data

Several complementary dust metrics were used because no single measure can characterize all aspects of Saharan dust–cloud interactions. The independently identified Saharan dust events (SDEs) provide an event-based framework for analysing cloud and radiative anomalies associated with validated dust intrusions. MERRA-2 dust column mass density was used as a continuous measure of the total atmospheric dust burden, allowing cloud properties to be related quantitatively to variations in dust loading. The threshold-based analysis extends this approach by progressively selecting days exceeding different column-dust levels, thereby characterizing dust-load-dependent cloud responses and their evolution across consecutive five-year periods without relying on a single arbitrary dusty-day threshold. Finally, vertically resolved MERRA-2 dust mass mixing ratios at 7–12 km were used to determine whether mineral dust was actually present at cirrus-relevant altitudes and whether cloud properties were more closely associated with upper-tropospheric dust than with total-column loading. Thus, these metrics address complementary aspects of the problem – event occurrence, total dust burden, dust-load dependence, and vertical dust–cloud co-occurrence – rather than representing alternative definitions of the same quantity.

2.2.1 Saharan dust events and column dust-loading thresholds

Saharan dust intrusion events were identified using a multistage methodology consistent with previous studies, through which several hundred Saharan dust outbreaks have been documented between 1979 and the present (Varga, 2020; Varga et al., 2013). The existing database was further extended and updated within the framework of the present study. Potential dust events were initially screened using daily aerosol index (AI) datasets derived from NASA's Ozone Monitoring Instrument observations and MERRA-2 dust column mass density, which are well suited for detecting elevated concentrations of atmospheric mineral aerosols. The identified candidate events were subsequently validated using multiple independent data sources. Saharan origin was confirmed through the analysis of satellite imagery and backward air-mass trajectory calculations performed with the HYbrid Single-Particle Lagrangian Integrated Trajectory (HYSPLIT) model, which enabled the determination of source regions and transport pathways (Stein et al., 2015).

Saharan dust events were investigated using data from the NASA Modern-Era Retrospective Analysis for Research and Applications Version 2 (MERRA-2) reanalysis. Atmospheric dust loading was characterized using hourly dust column mass density fields. Spatial and temporal variations in dust transport were analysed using country-scale mean values. The presence of mineral dust within the atmospheric column and its quantitative characterization were verified using the mapped (spatially represented) dust column mass density data from the MERRA-2 reanalysis. The synoptic meteorological background of individual events was analysed using NCEP/NCAR reanalysis data, focusing primarily on the 700 and 500 hPa geopotential height fields and the associated zonal and meridional wind components (for a detailed methodological description see (Varga, 2020)).

Beyond the analysis of discrete dust events, the relationship between atmospheric dust loading and cloud properties was investigated using continuous dust column mass density thresholds. In this approach, progressively restrictive dust-loading thresholds were applied. Because no universally accepted threshold exists for distinguishing dusty and non-dusty conditions across different geographical and climatic environments, and seasons, multiple dust-loading thresholds were applied. Dust column mass density threshold values were systematically varied between 0 and 0.006 g m^{-2} in in-

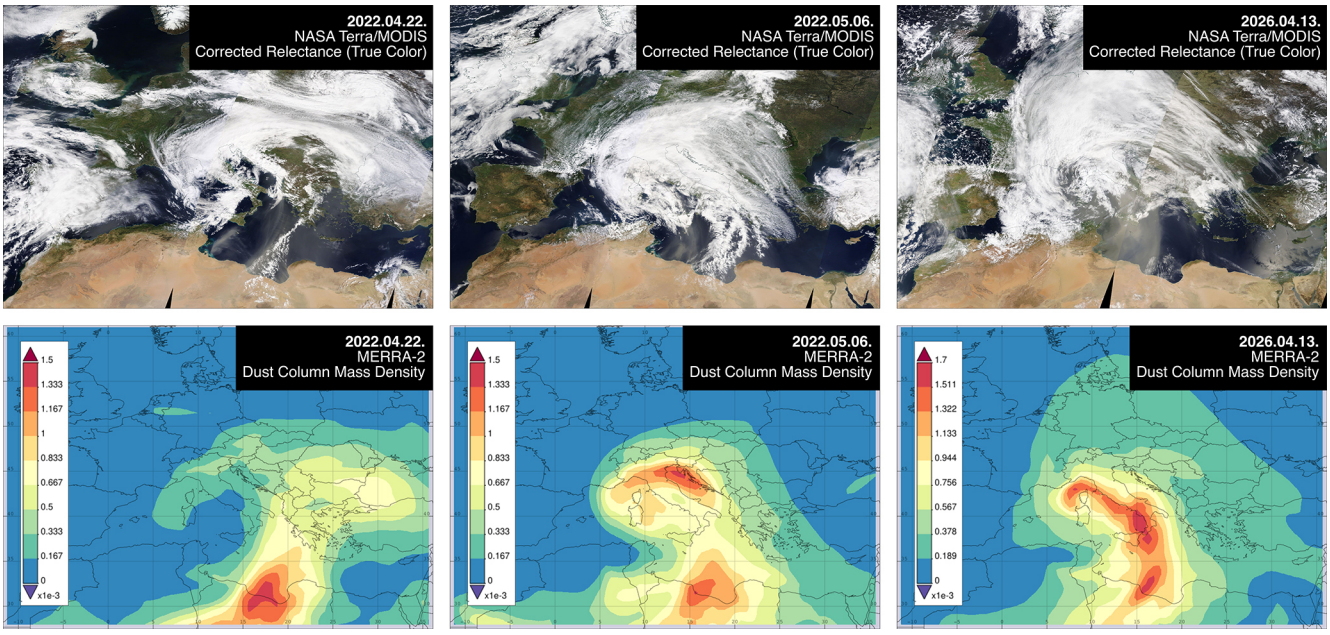


Figure 1. Examples of extensive upper-level cloud shields associated with Saharan dust transport over Europe on 22 April 2022, 6 May 2022, and 13 April 2026. Upper panels show NASA Terra/MODIS true-colour imagery, while lower panels show the corresponding MERRA-2 dust column mass density distributions. The illustrated cloud structures exhibit similarities to dust-infused baroclinic storm systems, although their classification and vertical dust–cloud overlap are not established by these images alone. The 2026 case is included for illustration and is not part of the 2001–2025 statistical analysis (sources: NASA Terra/MODIS – NASA WorldView; MERRA-2 dust column mass density – NASA's Global Modeling and Assimilation Office).

crements of 0.0001 g m^{-2}. For each threshold value, daily mean cloud parameters, including cirrus reflectance, high cloud cover fraction, and effective ice particle radius, were calculated and subsequently analysed seasonally within consecutive five-year time windows across the 2001–2025 study period.

This approach enabled the assessment of how different dust-loading regimes are associated with changes in the optical and spatial characteristics of cirrus clouds. To evaluate radiative impacts, the same methodology was applied to ice cloud effective particle radius, cloud fractions (at different heights), outgoing longwave radiation (OLR) data, allowing the investigation of long-term relationships between atmospheric dust loading, cirrus cloud development, and upper-tropospheric radiative processes. While this total-column threshold analysis provides a complementary view of dust-load-dependent cloud variability over the full daily record, the event-based analysis described below focuses specifically on the 276 independently identified SDEs and uses vertically resolved dust information to assess whether mineral dust was present at cirrus-relevant altitudes.

2.2.2 Dust column mass and upper-tropospheric dust

To assess whether Saharan dust was present at altitudes relevant to cirrus formation, the total-column analysis was complemented with three-dimensional MERRA-2 aerosol fields. For each of the identified SDEs, 3-hourly dust mass mixing ratios for the five MERRA-2 dust size bins (DU001–DU005) were extracted over the study domain from the native model-level aerosol product. Total dust mass mixing ratio (kg kg^{-1}) was calculated as the sum of the five size bins. Aerosol fields were matched to the corresponding three-dimensional MERRA-2 atmospheric fields, and the geometric height assigned to each model level was used to determine the actual altitude of the dust at every time step and grid point. This allowed the dust distribution to be evaluated independently of fixed model-level or pressure-level assumptions. Upper-tropospheric dust was primarily characterized over the 7–12 km altitude range, with additional calculations for the 7–8, 8–9, 9–10, and 10–12 km layers to examine the vertical dependence of the dust–cirrus relationship. Event-level mean dust mass mixing ratios were calculated from all grid points and 3-hourly time steps falling within each altitude interval. These vertically resolved dust metrics were subsequently compared with the MODIS and HIRS cloud properties used in the original analysis to determine whether cirrus responses were more closely associated with dust present at cirrus-relevant altitudes than with total-column dust loading.

2.3 Cloud and other atmospheric parameters

In addition to atmospheric dust loading, several satellite- and reanalysis-based datasets were employed to investigate the

long-term variability of cloud physical properties and radiative processes. Thermodynamic and cloud cover parameters of high-level clouds were obtained from the MERRA-2 reanalysis produced by NASA's Global Modeling and Assimilation Office. The cloud top pressure and cloud top temperature variables were used to characterize the vertical position and thermal properties of upper-level clouds, while the low, middle, and high cloud cover fraction datasets were used to assess seasonal and long-term variations in cloud cover at different atmospheric levels. MERRA-2 is a global atmospheric reanalysis based on the Goddard Earth Observing System Model Version 5 (GEOS-5), incorporating both satellite and in situ observations through data assimilation.

To investigate the optical and microphysical properties of cirrus clouds, Level-3 products from the Moderate Resolution Imaging Spectroradiometer (MODIS) sensors onboard NASA's Terra and Aqua satellites were utilized. Cloud fraction is defined as the fraction of a model grid cell covered by clouds within a specified atmospheric layer, ranging from 0 (cloud-free) to 1 (completely cloud-covered). In MERRA-2, low-, middle-, and high-level cloud fractions correspond to clouds occurring between the surface and 700, 700 and 400 hPa, and above 400 hPa, respectively. These pressure ranges approximately correspond to altitudes of 0–3, 3–7, and >7 km, although their actual geometric heights vary with atmospheric conditions. The cirrus reflectance dataset was used to characterize variations in the optical reflectivity of high-level ice clouds, while the ice cloud effective particle radius variable provided estimates of the effective size of ice crystals within cirrus clouds. (MODIS-derived effective ice-particle radii are subject to retrieval uncertainties associated with cloud optical thickness, ice crystal shape assumptions, and cloud heterogeneity, which should be considered when interpreting small differences of a few micrometres, particularly in long-term comparisons.) The Terra satellite has provided global observations since 1999, while Aqua has been operational since 2002, delivering continuous measurements of atmospheric and cloud properties.

OLR was analysed using data from the High-resolution Infrared Radiation Sounder (HIRS) satellite instrument. OLR represents the amount of longwave radiation emitted from the Earth–atmosphere system to space and is highly sensitive to the presence of high, cold cloud tops. Consequently, HIRS OLR observations provide a suitable basis for assessing the radiative impacts of dust-associated cirrus clouds and for examining their long-term variability over the study region.

2.4 Event-based statistical analysis

The statistical analysis was based on 276 distinct Saharan dust events (SDEs) identified during 2001–2025. Individual events occasionally extended over several consecutive days; however, each multi-day episode was treated as a single observational unit, using event-aggregated atmospheric variables. Thus, the sample size of 276 refers to independent dust episodes rather than individual dusty days. The seasonal and five-year event counts are summarized in Table 1. Rather than relying primarily on correlations between dust concentration and individual cloud parameters, the analysis was designed to compare cloud states associated with SDEs against low-dust background conditions. For the five-year comparisons, the high-Dust7–12 SDE subsets were defined using the season-specific median thresholds calculated from the complete 2001–2025 SDE dataset. These thresholds were kept constant across the five consecutive periods to ensure a consistent classification of upper-tropospheric dust abundance. Low-dust reference conditions were identified using the fixed 75th-percentile threshold of the complete daily dust column distribution, excluding identified SDE days. For each five-year period, only reference days belonging to the corresponding period and season were included in the comparison. This criterion yielded 6836 reference days and excluded the upper quartile of the total-column dust distribution, where substantial dust influence was more likely. All comparisons were performed separately for winter, spring, summer, and autumn to account for the pronounced seasonal variability in both Saharan dust transport and cloud conditions.

To examine whether the vertical penetration of dust into the upper troposphere was associated with the magnitude of the cloud response, SDEs were additionally divided within each season according to their Dust7–12 values. Events below or equal to the seasonal median Dust7–12 concentration were classified as lower-upper-tropospheric-dust SDEs, whereas events above the seasonal median were classified as higher-upper-tropospheric-dust SDEs. The use of season-specific thresholds avoided applying a single concentration criterion to seasons characterized by substantially different upper-tropospheric dust distributions. Three complementary contrasts were then evaluated: (i) all SDE days versus low-dust reference days, (ii) lower- and higher-Dust7–12 SDE subsets separately versus the corresponding seasonal reference, and (iii) higher- versus lower-Dust7–12 SDEs directly. The latter comparison was used to determine whether cloud properties differed systematically among SDEs depending on the amount of mineral dust present at 7–12 km.

The analysis included cirrus reflectance, effective ice particle radius, low-, mid-, and high-level cloud fraction, cloud-top pressure, cloud-top temperature, and OLR. Because several variables exhibited non-normal distributions and unequal group sizes, group differences were evaluated using two-sided Mann–Whitney U tests (Mann and Whitney, 1947). The magnitude and direction of the differences were quantified using rank-biserial correlation (r_{rb}) as a non-parametric effect-size measure, with positive values indicating higher values in the first group and negative values indicating lower values. To control for multiple comparisons, p-values were adjusted using the Benjamini–Hochberg false discovery rate (FDR) procedure, with FDR-adjusted ($q < 0.05$) considered statistically significant (Ben-

Table 1. Seasonal and total frequency and intensity of Saharan dust events (SDEs) over the Carpathian Basin during the 2001–2025 period.

	Winter		Spring		Summer		Autumn		Total	
Timeframe	SDEs	Dust mass	SDEs	Dust mass	SDEs	Dust mass	SDEs	Dust mass	SDEs	Dust mass
	(n)	(avg.) [g m^{-2}]	(n)	(avg.) [g m^{-2}]	(n)	(avg.) [g m^{-2}]	(n)	(avg.) [g m^{-2}]	(n)	(avg.) [g m^{-2}]
2001–2005	3	0.009	18	0.011	11	0.007	8	0.005	40	0.009
2006–2010	12	0.006	18	0.007	10	0.005	8	0.005	48	0.006
2011–2015	12	0.006	25	0.007	16	0.003	7	0.004	60	0.005
2016–2020	10	0.004	26	0.008	16	0.003	9	0.005	61	0.006
2021–2025	5	0.006	29	0.008	19	0.007	14	0.005	67	0.007
Total	42	0.006	116	0.008	72	0.005	46	0.005	276	0.006

jamini and Hochberg, 1995). Group medians were used to characterize the magnitude of the observed differences.

Because vertically resolved Dust7–12 data were available only for the 276 SDE days, upper-tropospheric dust concentrations could not be directly compared between SDE and reference days. Accordingly, the low-dust reference group was defined independently using total-column dust mass, whereas Dust7–12 was used specifically to stratify the SDE population according to the degree of upper-tropospheric dust presence. This design therefore tests whether the cloud state associated with SDEs differs from low-dust background conditions and, more specifically, whether these anomalies become more pronounced when larger amounts of mineral dust are present at cirrus-relevant altitudes.

3 Results

3.1 Frequency and synoptic types of Saharan dust events

A total of 276 Saharan dust events (SDEs) were identified over the Carpathian Basin during the 2001–2025 study period (Table 1, Fig. 2). The seasonal distribution of events was strongly asymmetric, with spring accounting for the highest number of dust intrusions (116 events), representing approximately 42 % of all identified cases. The spring maximum was followed by summer with 72 events, while 46 and 42 events were recorded during autumn and winter, respectively. Mean dust loading was also highest during spring, reaching 0.008 g m^{-2}, whereas average dust column mass density values ranged between 0.005 and 0.006 g m^{-2} in the remaining seasons.

Analysis of consecutive five-year periods revealed a clear increasing trend in the frequency of dust events. While 40 events were identified during 2001–2005, the number increased to 48 during 2006–2010, 60 during 2011–2015, 61 during 2016–2020, and 67 during 2021–2025. This corresponds to an increase of nearly 70 % relative to the beginning of the study period. The increase was primarily driven by a growing number of spring and summer dust outbreaks. Spring events increased from 18 to 29 cases, while summer events rose from 11 to 19. Autumn also exhibited a moderate increase, from 8 to 14 events, whereas winter dust intrusions showed no clear long-term trend.

In contrast, the intensity of dust loading did not display a similarly pronounced increase. Average dust column mass density values remained within a relatively narrow range of 0.005–0.009 g m^{-2} throughout the different five-year periods. These results suggest that the observed long-term changes are primarily associated with an increasing frequency of Saharan dust intrusions rather than a systematic intensification of individual events. The strongest seasonal signal remained evident during spring, which exhibited both the highest event frequency and the greatest average dust loading, highlighting the dominant role of the spring season in Central European dust transport and related atmospheric processes.

The classification of events according to their synoptic background revealed substantial differences in dust transport characteristics and associated cloud properties. Type 1 events are characterized by a pronounced pressure gradient between a deep trough over the eastern North Atlantic and a high-pressure system extending across the Mediterranean and North Africa. In many cases, cut-off lows detached from the parent trough trigger intense dust storms within the intramontane basins of the Atlas Mountains, and in the forefront of the mountain range. The resulting dust plumes are subsequently transported toward Central Europe by southwesterly flow.

Type 2 events are associated with Mediterranean cyclones, during which dust is advected into the study region within the warm sector and ahead of the cyclone. (The Saharan dust events illustrated in Fig. 1 are representative examples of Type 2 synoptic situations, characterized by dust transport associated with Mediterranean cyclones.) Type 3 events are characterized by the longest transport pathways. In these cases, an anticyclonic circulation over the northwestern Sahara transports dust from western Saharan source regions to-

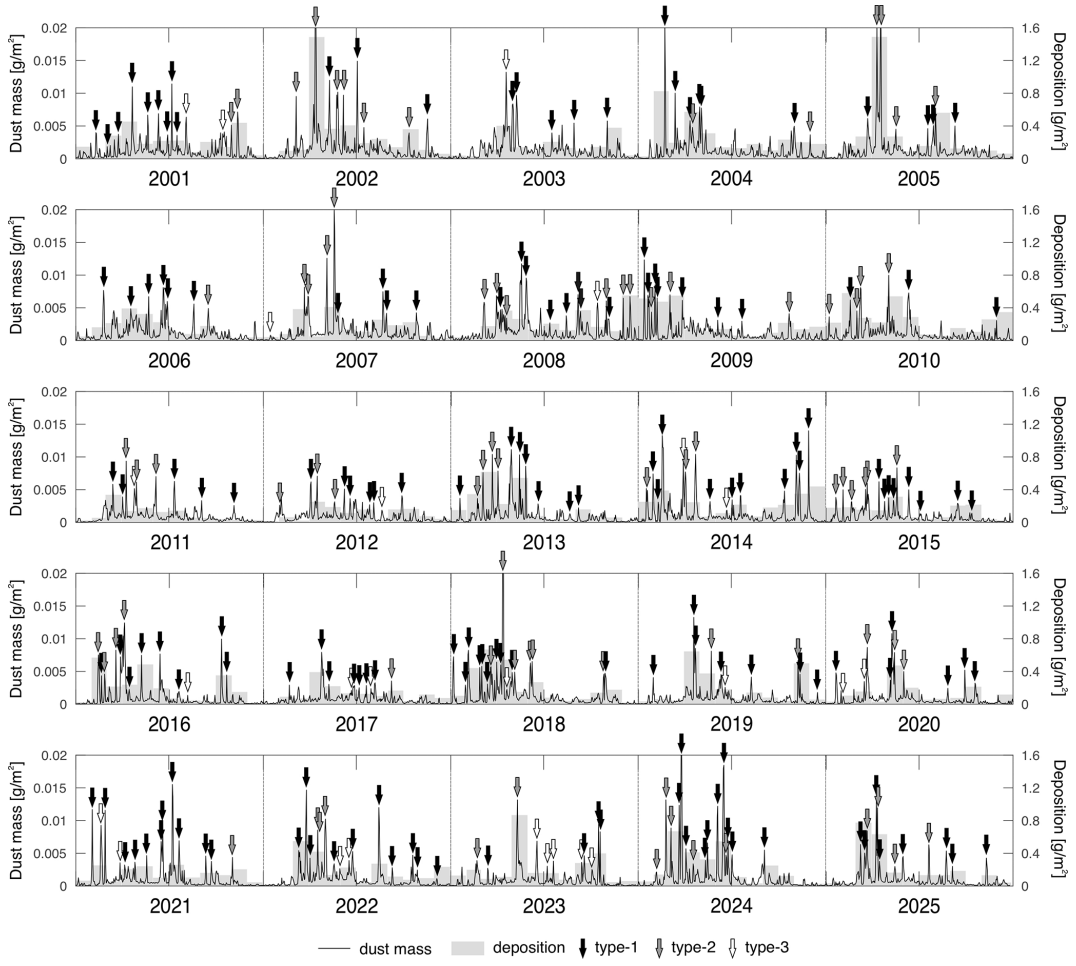


Figure 2. Temporal evolution of atmospheric dust loading, dust deposition, and the frequency and synoptic classification of Saharan dust events over the Carpathian Basin during the 2001–2025 period. (Type-1, type-2, and type-3 refer to the synoptic types of dust storm events described in the text.)

ward the eastern and northeastern Atlantic, from where prevailing westerlies subsequently carry the aerosol plume toward Central Europe.

Considering the entire study period, Type 1 represented the most frequent synoptic category with 101 identified events. Type 2 accounted for 53 events, whereas only 9 cases were classified as Type 3. The highest average dust loading was observed for Type 2 events (0.011 g m^{-2}), while Type 1 and Type 3 episodes exhibited similar mean dust column mass density values of approximately 0.007–0.008 g m^{-2}.

3.2 Relationship between atmospheric dust and cloud formation processes

3.2.1 Synoptic types of SDEs and high-level cloud properties

The characteristics of high-level cloud cover revealed clear differences among the three synoptic categories. The highest mean high cloud fraction was observed for Type 2 events (0.62), while somewhat lower values were associated with Type 1 situations (0.52), and substantially lower high-cloud coverage characterized Type 3 events (0.31). Similar differences were found for cirrus reflectance. The mean reflectance of Type 2 events (0.22) was approximately twice that observed for Type 1 events (0.10), whereas Type 3 situations exhibited extremely low reflectance values (0.017). Among the three synoptic categories, Type 2 events were associated with the highest high-cloud fractions and cirrus reflectance.

The effective radius of ice crystals also exhibited substantial differences among the synoptic categories. The smallest mean particle sizes were associated with Type 2 events (29.5 µm), while larger effective radii occurred during Type 1 and especially Type 3 situations.

The importance of synoptic conditions also changed over time. The frequency of Type 1 situations increased throughout the study period, particularly during 2011–2015, while Type 2 events remained frequent during the most recent years. Concurrently, both dominant synoptic categories ex-

hibited increasing high cloud cover fractions and cirrus reflectance values. These temporal differences indicate that the cloud properties associated with the dominant synoptic categories have varied over the study period, although they do not by themselves demonstrate changes in the efficiency of cirrus formation. Owing to its low occurrence frequency and comparatively weak cloud-related characteristics, Type 3 appears to be of secondary importance in terms of dust–cirrus interactions.

3.2.2 Upper-tropospheric dust occurrence and comparison with column dust loading

The vertically resolved MERRA-2 analysis showed that mineral dust was frequently present at cirrus-relevant altitudes during the identified SDEs. Across the 276 events, the median event-mean dust mass mixing ratio in the 7–12 km layer was 9.63×10^{-9} kg kg^{-1} (Fig. 3). Upper-tropospheric dust was not restricted to the lower part of this altitude range: the corresponding median was 8.33×10^{-9} kg kg^{-1} at 8–12 km and 4.37×10^{-9} kg kg^{-1} at 10–12 km. Of all SDEs, 264 (95.7 %) exhibited event-mean dust mass mixing ratios exceeding 10^{-9} kg kg^{-1} between 7 and 12 km, while 204 (73.9 %) exceeded 5×10^{-9} kg kg^{-1}, and 134 (48.6 %) exceeded 10^{-8} kg kg^{-1}. Even when the analysis was restricted to 8–12 km, these thresholds were exceeded in 93.1 %, 67.0 %, and 44.6 % of the events, respectively. At 10–12 km, 81.2 % of the SDEs still exceeded 10^{-9} kg kg^{-1}.

The amount of dust at 7–12 km was also substantial relative to that at 3–7 km; the upper-tropospheric mean reached at least 30 % of the 3–7 km value in 62 % of the events and at least 50 % in 35.5 % of the events. These results demonstrate that, within MERRA-2, Saharan dust during the investigated events was generally not confined to the lower and middle troposphere but frequently extended into the altitude range occupied by upper-level ice clouds.

3.2.3 Seasonal cloud-property differences associated with upper-tropospheric dust during SDEs

The event-based analysis revealed pronounced seasonal differences in cloud and radiative properties between Saharan dust events and low-dust reference conditions (Table 2). The differences were particularly marked for SDEs characterized by above-median dust concentrations in the 7–12 km layer. Across all seasons, these high-Dust7–12 events were associated with significantly enhanced cirrus reflectance and high-cloud fraction, together with substantially lower cloud-top pressure and temperature. Most of these differences remained highly significant after FDR correction and were accompanied by moderate to large rank-biserial effect sizes.

The largest overall contrasts were observed during winter and spring. In winter, high-Dust7–12 SDEs showed particularly large differences in high-cloud fraction, cloud-top properties, and OLR relative to low-dust reference conditions.

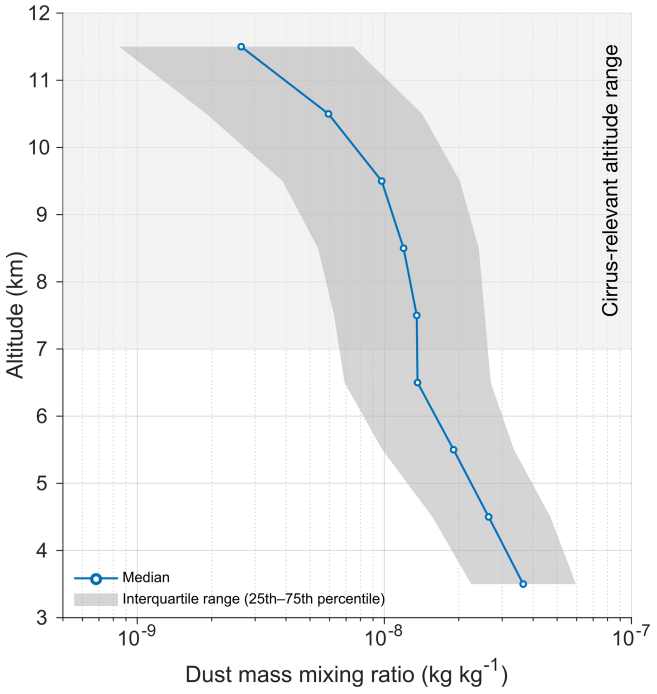


Figure 3. Vertical distribution of Saharan dust during the 276 identified SDEs. (The line shows the median MERRA-2 dust mass mixing ratio, with the shaded envelope representing the interquartile range, while the shaded 7–12 km layer indicates cirrus-relevant altitudes.)

Spring exhibited a similarly coherent pattern, with enhanced cirrus reflectance and high-cloud fraction and reduced cloud-top pressure, cloud-top temperature, and OLR. A significant reduction in effective ice particle radius was also detected in spring, whereas particle-size differences were not statistically significant in the other seasons. Summer exhibited smaller cirrus and radiative differences, although high-cloud fraction and cloud-top properties remained significantly different from reference conditions. During autumn, the largest differences were observed in high-cloud fraction and cloud-top pressure and temperature.

Direct comparison of SDEs with above- and below-median Dust7–12 concentrations showed that the differences were not restricted to the contrast between SDE and reference conditions. Higher upper-tropospheric dust concentrations within SDEs were accompanied by significantly greater cirrus reflectance and high-cloud fraction during winter and spring. Spring high-Dust7–12 events additionally showed significantly smaller effective ice particle radii and lower OLR than lower-Dust7–12 events. During summer, the most pronounced within-SDE difference occurred in high-cloud fraction, whereas autumn showed the clearest differences in cloud-top pressure and temperature. Thus, the seasonal analysis identified distinct cloud-property differences not only between SDEs and low-dust background conditions but also

according to the amount of mineral dust present within the 7–12 km layer during the events.

A separate within-SDE comparison was performed to determine whether cloud properties differed according to upper-tropospheric dust abundance independently of the SDE–background contrast. For this analysis, SDEs with above-seasonal-median Dust7–12 concentrations were compared directly with SDEs below or equal to the corresponding seasonal median.

In winter, median cirrus reflectance was 0.183 in the higher-Dust7–12 group compared with 0.068 in the lower-Dust7–12 group, while high-cloud fraction was 0.810 and 0.610, respectively. Cloud-top temperature decreased from 233.9 to 223.8 K and OLR from 199.9 to 172.0 $\mathrm{W\,m^{-2}}$; all four differences remained significant after FDR correction. In spring, cirrus reflectance increased from 0.079 to 0.167 and high-cloud fraction from 0.565 to 0.708 between the lower- and higher-Dust7–12 subsets. Effective ice particle radius decreased significantly, from 31.90 to 28.44 µm ($r_{\mathrm{rb}} = -0.36$, $q = 0.0023$), while OLR decreased from 215.0 to 192.6 $\mathrm{W\,m^{-2}}$ ($r_{\mathrm{rb}} = -0.44$, $q < 0.001$). During summer, the principal significant within-SDE difference was observed for high-cloud fraction (0.199 versus 0.497, $r_{\mathrm{rb}} = 0.50$, $q < 0.001$), whereas autumn showed significant differences primarily in cloud-top pressure (405 versus 278 hPa, $r_{\mathrm{rb}} = -0.57$, $q = 0.0022$) and cloud-top temperature (238.1 versus 228.0 K, $r_{\mathrm{rb}} = -0.54$, $q = 0.0035$).

3.3 Long-term trends of dust and cirrus cloud relationships in spring

Based on the seasonal analysis above, the long-term assessment was focused on spring, which combined the largest number of identified SDEs and the highest mean dust loading with the most coherent dust-dependent responses across cirrus reflectance, high-cloud fraction, cloud-top properties, and OLR.

The five-year analysis revealed substantial temporal variability in springtime SDE-associated cloud properties without a corresponding monotonic increase in upper-tropospheric dust loading. Median Dust7–12 during spring SDEs varied between 6.73×10^{-8} and 1.29×10^{-7} $\mathrm{kg\,kg^{-1}}$, with the lowest value occurring in 2016–2020 and no systematic increase towards the end of the record. In contrast, the descriptive comparison of five-year median values indicated a pronounced increase in the cirrus-reflectance anomaly associated with high-Dust7–12 SDEs. Relative to the corresponding low-dust reference conditions, median cirrus reflectance was 143 % higher in 2001–2005 and 398 % higher in 2021–2025. These values describe differences between the investigated five-year subsets and should not be interpreted as evidence of a statistically significant temporal trend, as uncertainty estimates for the between-period changes were not calculated. The absolute median cirrus reflectance increased from 0.116 in 2001–2005 to 0.223 in 2021–2025, while the corresponding background values remained similar (0.048 and 0.045, respectively).

Other cloud properties showed persistent but less monotonic differences. High-cloud fraction during high-Dust7–12 SDEs was 122 %–161 % above background during 2001–2015, 54 % higher in 2016–2020, and 135 % higher in 2021–2025. Cloud-top pressure remained 25 %–34 % lower and cloud-top temperature approximately 5 %–7 % lower than background throughout the five periods, with the largest recent differences occurring in 2021–2025. Effective ice particle radius showed greater temporal variability: the anomaly changed from +2.8 % in 2001–2005 to −15.7 % in 2006–2010, −8.3 % in 2011–2015, approximately zero in 2016–2020, and −7.7 % in 2021–2025. OLR remained lower during high-Dust7–12 SDEs in every period, with differences ranging from approximately −10 % to −17 %. Thus, among the investigated variables, the clearest five-year change was observed in cirrus reflectance, whose SDE-associated enhancement became substantially larger over the study period despite the absence of a parallel increase in Dust7–12.

As a complementary analysis independent of the vertically resolved SDE stratification, the longer-term behaviour was also examined using progressively restrictive total-column dust-loading thresholds applied to the complete daily dataset (Fig. 4). Middle- and high-level cloud cover fractions generally increase with increasing dust column mass density, whereas low-cloud fraction shows neither a consistent dust-load dependence nor a systematic temporal pattern. The relationship is most pronounced for high clouds, for which higher dust-loading thresholds are associated with larger cloud fractions in nearly all five-year periods. Differences among the periods are also evident, with the largest high-cloud fractions occurring under the highest dust-loading conditions in the later part of the record. During 2021–2025, high-cloud fractions associated with the highest dust loads were approximately 1.5 times those observed during 2001–2005.

Cloud-top pressure and cloud-top temperature also show marked variations across the dust-loading thresholds. Higher dust column mass densities are generally associated with lower cloud-top pressures and lower cloud-top temperatures, indicating a shift towards higher and colder cloud tops. These differences are particularly pronounced during 2011–2015 and 2021–2025. The simultaneous increase in high-cloud fraction and decrease in cloud-top pressure and temperature is therefore a consistent feature of the higher dust-loading subsets, although the magnitude of the response varies among the five-year periods.

The strongest dust-load-dependent changes among the cirrus-specific properties are observed for cirrus reflectance and effective ice-particle radius. In spring, cirrus reflectance increases towards higher dust-loading thresholds during all five-year periods, but both the magnitude and range of the response differ substantially among periods. The largest reflectance values at elevated dust loads occur during 2016–

Table 2. Relative changes in cloud and radiative properties during high-Dust7–12 SDEs compared with low-dust reference conditions.

Season	Cirrus reflectance	High cloud fraction	Effective ice cloud radius	Cloud top pressure	Cloud top temperature	OLR
Winter	+194.5 %***	+146.5 %***	−4.9 % n.s.	−44.0 %***	−8.8 %***	−16.1 %***
Spring	+272.0 %***	+133.2 %***	−7.2 %**	−30.0 %***	−5.5 %***	−14.4 %***
Summer	+99.3 %***	+94.7 %***	0.0 % n.s.	−34.8 %***	−6.6 %***	−4.6 %*
Autumn	+160.9 %**	+119.7 %***	−4.8 % n.s.	−41.4 %***	−7.2 %***	−8.6 %*

Values represent percentage differences between median cloud properties during SDEs with above-seasonal-median Dust7–12 concentrations and the corresponding low-dust reference conditions, calculated relative to the reference median. Statistical significance is based on two-sided Mann–Whitney U tests with Benjamini–Hochberg FDR correction: * $q < 0.05$, ** $q < 0.01$, *** $q < 0.001$; n.s., not significant.

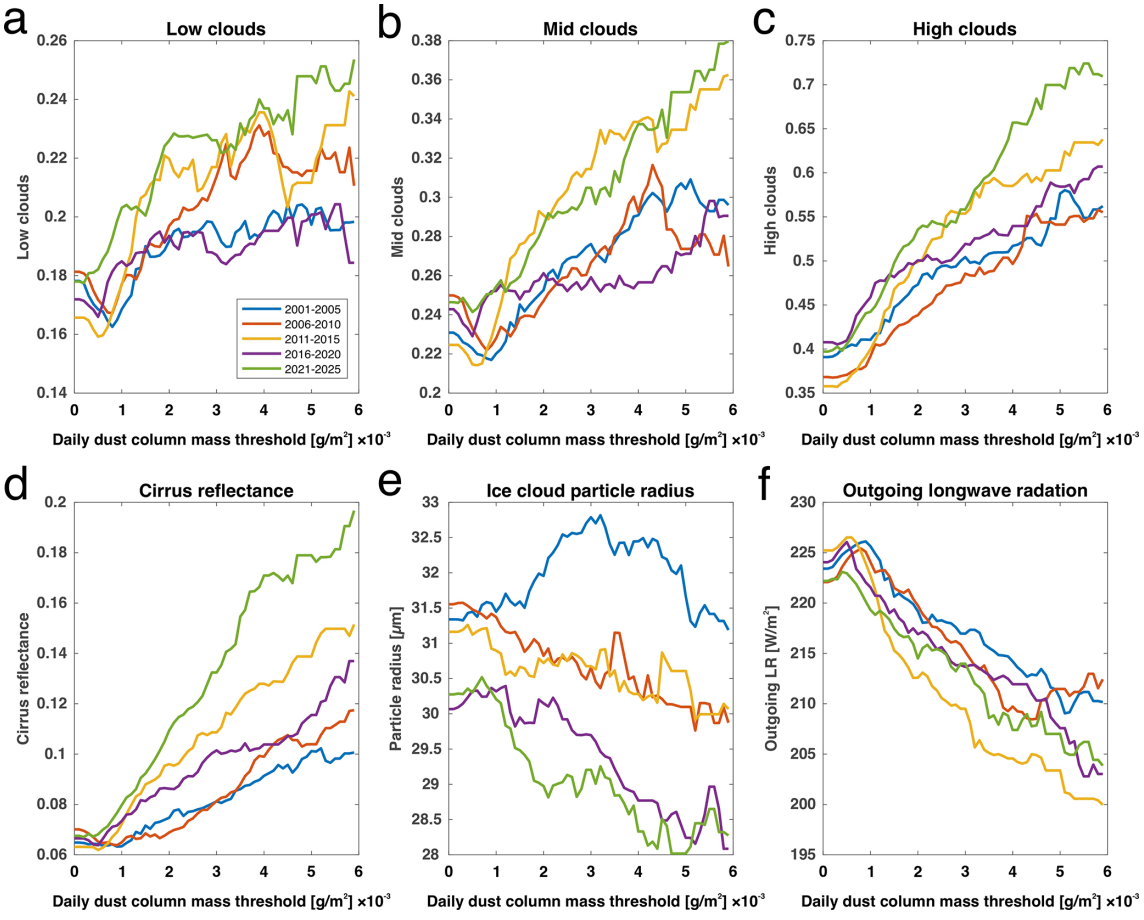


Figure 4. Variations in the investigated atmospheric and cloud-physical parameters as a function of daily dust column mass density thresholds during 2001–2025, presented for consecutive five-year periods. Panels show **(a)** low-, **(b)** middle-, and **(c)** high-level area-averaged cloud fractions, **(d)** cirrus reflectance, **(e)** ice-cloud effective particle radius, and **(f)** outgoing longwave radiation.

2020 and 2021–2025. Effective ice-particle radius shows an opposite pattern, with smaller values generally occurring at higher dust-loading thresholds. Thus, the highest dust-loading subsets are characterized by a combination of enhanced cirrus reflectance and reduced effective ice-particle radius. As with the other cloud variables, however, the magnitude of these differences is not uniform across the five five-year periods.

3.4 Radiative effects of dust-associated clouds

To investigate the radiative impacts of dust-associated high-level clouds, HIRS OLR data were analysed for the spring season. Under the highest dust-loading conditions, OLR values were approximately 15–25 W m^{-2} lower than those observed during low-dust situations. These findings are consistent with the changes observed in cloud top pressure

and cloud top temperature, which indicate that higher dust-loading conditions are associated with higher-altitude and colder ice-cloud systems. The simultaneous increase in high cloud fraction and cirrus reflectance further suggests that dust-rich conditions favour the development of more extensive and optically thicker upper-level cloud cover. From a radiative perspective, the observed decrease in OLR indicates that high, cold cirrus clouds retain a larger fraction of outgoing longwave radiation, thereby reducing the effective radiative emission of the surface–atmosphere system. Across all five-year periods, progressively higher dust-loading thresholds were associated with lower OLR values. The magnitude and absolute level of this response varied among periods, with particularly low OLR values under high dust-loading conditions during 2011–2015 and 2016–2020. These results demonstrate a persistent dust-load dependence of springtime OLR, but do not indicate a uniform monotonic strengthening of the relationship over the full 25-year period.

It should be noted that the observed OLR response cannot be attributed exclusively to dust-associated changes in cirrus, because mineral dust itself contributes to the longwave radiative balance. The OLR variations are therefore interpreted here as an integrated radiative signature associated with dust-loading conditions rather than as an isolated cirrus radiative effect.

4 Discussion

4.1 Upper-tropospheric dust occurrence and cloud response during Saharan dust events

Although long-range Saharan dust transport over Europe is most commonly associated with the lower and middle troposphere, with elevated dust layers frequently occurring at approximately 3–4 km altitude (Ansmann et al., 2003; Seifert et al., 2010), this typical transport level should not be interpreted as an upper limit to the vertical extent of mineral dust. Saharan dust can also be transported to substantially higher levels, particularly when strong convective uplift over the source regions, frontal lifting, or large-scale ascending motion is involved. Consequently, dust layers and detectable mineral dust have repeatedly been observed in the upper troposphere, including at altitudes approaching or overlapping those characteristics of cirrus clouds (Ansmann et al., 2019; Weger et al., 2018; Seifert et al., 2023). Such vertical transport is particularly relevant for cirrus formation because mineral dust can provide INPs capable of initiating heterogeneous ice nucleation under suitable thermodynamic conditions (DeMott et al., 2003; Kärcher et al., 2022). Our vertically resolved results are consistent with this picture: although the largest dust amounts are generally expected at lower altitudes, dust was frequently present between 7 and 12 km during the investigated SDEs. In particular, 95.7 % of the events exhibited mean dust mass mixing ratios above 10^{-9} kg kg^{-1} at 7–12 km, and 81.2 % still exceeded this threshold at 10–12 km. Thus, the predominance of Saharan dust transport at lower and middle tropospheric levels does not preclude regular dust occurrence at cirrus-relevant altitudes over Central Europe. This vertical overlap provides an important physical prerequisite for the statistical dust–cirrus relationships identified in the present study, although it does not by itself establish a causal ice-nucleation effect.

The vertically resolved analysis provides a more physically constrained perspective on the relationship between Saharan dust and upper-level clouds than comparisons based solely on total-column dust loading. The amount of dust integrated over the entire atmospheric column does not necessarily represent the aerosol population available at cirrus-forming altitudes, because a substantial fraction of transported mineral dust may remain confined to the lower and middle troposphere. By specifically distinguishing SDEs according to dust abundance within the 7–12 km layer, the present analysis shows that the most pronounced upper-level cloud anomalies tend to occur when substantial amounts of mineral dust are present at these altitudes.

Compared with low-dust background conditions, SDEs with above-median Dust7–12 concentrations were characterized by substantially enhanced cirrus reflectance and high-cloud fraction in all seasons, together with systematically higher and colder cloud tops. The magnitude of these differences was considerable: cirrus reflectance was approximately 99 %–272 % higher and high-cloud fraction approximately 95 %–147 % higher, depending on season. The corresponding large effect sizes for several cloud-top and high-cloud parameters indicate that these differences cannot be attributed merely to the large number of background observations. The accompanying reduction in OLR, particularly during winter and spring, is also consistent with the greater occurrence of high, cold clouds during these events.

Importantly, the differences were not limited to the contrast between SDEs and low-dust background conditions. Stratification of the 276 SDEs according to their upper-tropospheric dust abundance showed that events with higher Dust7–12 concentrations frequently exhibited more pronounced cloud anomalies than SDEs containing less dust at these altitudes. This distinction is important because both subsets consist of independently identified Saharan dust events. Thus, differences between them cannot be explained simply by the presence or absence of a Saharan air mass. Instead, the results indicate that the vertical distribution of dust within the troposphere is associated with the magnitude and type of the observed cloud response.

The winter and spring results are particularly noteworthy. During winter, higher-Dust7–12 SDEs showed markedly greater cirrus reflectance and high-cloud fraction, together with colder cloud tops and lower OLR than lower-Dust7–12 events. Spring exhibited a similarly coherent response, but additionally showed a significant reduction in effective ice particle radius. In high-Dust7–12 spring SDEs, the me-

dian effective radius was approximately 7 % smaller than under low-dust reference conditions and was also significantly smaller than during lower-Dust7–12 SDEs. The simultaneous occurrence of enhanced cirrus reflectance, increased high-cloud fraction, and reduced effective ice particle size is compatible with a microphysical response involving enhanced ice nucleation. Mineral dust is an efficient ice-nucleating aerosol, and an increased number of ice crystals could contribute to greater cloud reflectance while reducing characteristic particle size. However, the absence of a similarly robust radius response in the other seasons indicates that this mechanism cannot be inferred universally from the present observations.

The pronounced seasonal differences are also consistent with previous modelling studies demonstrating that the microphysical response of cirrus clouds to mineral dust depends strongly on the competition between heterogeneous and homogeneous ice nucleation, as well as on vertical velocity and ice supersaturation (Kärcher et al., 2022, 2023). Consequently, similar upper-tropospheric dust concentrations may be associated with different cloud properties under different meteorological conditions. This dependence provides an important context for interpreting the seasonal variability observed in our analysis. In summer, enhanced Dust7–12 was most clearly associated with increased high-cloud fraction, whereas autumn exhibited particularly pronounced differences in cloud-top pressure and temperature. Such differences are consistent with the strong dependence of ice-cloud formation on the thermodynamic and dynamical environment. Temperature, ice supersaturation, vertical motion, and moisture availability may determine whether mineral dust reaching 7–12 km can effectively participate in ice formation and how the resulting cloud field develops. The seasonal dependence therefore provides an important indication that the observed dust–cloud relationship is conditional on the atmospheric environment.

The vertically resolved results also help explain why relationships based on total-column dust loading were comparatively weak. Total-column dust combines aerosol located at very different altitudes, much of which may have limited relevance to upper-tropospheric ice-cloud formation. Consequently, a strong SDE can exhibit high column-integrated dust loading while containing relatively little mineral dust near cirrus-forming levels. Explicit consideration of Dust7–12 reduces this vertical mismatch and reveals substantially clearer differences between events characterized by relatively low and high upper-tropospheric dust abundance. This emphasizes the importance of representing aerosol vertical distribution, rather than column loading alone, when investigating mineral dust–cirrus interactions.

Nevertheless, the observed differences should not be interpreted as direct evidence of dust-induced ice nucleation. Saharan dust reaching the upper troposphere is transported by atmospheric circulation that simultaneously determines vertical motion, humidity, temperature, and cloud formation. The high-Dust7–12 and low-Dust7–12 SDE subsets may therefore also represent different meteorological regimes. The present results demonstrate that upper-tropospheric dust occurrence is closely associated with distinct cloud states, but separating direct aerosol microphysical effects from the meteorological conditions responsible for both vertical dust transport and cloud development requires additional thermodynamic and dynamical information.

The complementary total-column threshold analysis also indicated increasing middle-level cloud fraction at higher dust-loading thresholds, suggesting that the observed relationships are not restricted to the classical cirrus altitude range. This suggests that the influence of Saharan dust may extend beyond classical cirrus formation and potentially affect cloud systems developing within the mixed-phase temperature regime. The temporal evolution of the dust–cloud relationship cannot be interpreted solely in terms of changes in mineral-dust INPs availability. Cirrus nucleation and subsequent cloud development are also strongly controlled by the dynamical environment, including vertical velocity, wind shear, turbulence, and the associated variability in ice supersaturation. Recent observations of dusty cirrus and large-eddy simulations indicate that changes in turbulence and updraft strength can substantially modify ice crystal nucleation, cloud structure, and persistence even under comparable aerosol conditions (Juurikkala et al., 2026; Pieper et al., 2026). Thus, the observed changes in cirrus properties during Saharan dust events may reflect a combined influence of mineral-dust availability and concurrent changes in upper-tropospheric dynamics rather than an aerosol effect alone.

4.2 Evidence for changing dust–cloud relationships

The combined results indicate that the relationship between Saharan dust and upper-level cloud properties over Hungary has evolved during the past 25 years, although this evolution cannot be described as a uniform strengthening across all investigated variables. The clearest long-term change was found in cirrus reflectance, for which the SDE-associated anomaly increased substantially between the beginning and the end of the study period. Together with the increasing frequency of SDEs, this suggests that the long-term evolution involves both more frequent dust intrusions and changes in the optical properties of cirrus associated with high dust loading.

The consistency of the event-based comparisons strengthens this interpretation. SDEs with higher upper-tropospheric dust abundance showed more pronounced differences in several cloud properties not only relative to low-dust background conditions, but also relative to SDEs with lower Dust7–12 concentrations. This distinction is important because the latter comparison is restricted entirely to independently identified Saharan dust events and therefore specifically addresses differences associated with the amount of dust reaching cirrus-relevant altitudes. The strongest and

most coherent contrasts occurred in winter and spring, while their magnitude and the affected cloud properties varied among seasons.

The pronounced seasonal dependence, particularly the coherent response observed in spring, further suggests that the effect associated with dust depends on the thermodynamic state of the atmosphere. Mineral dust can provide efficient INPs, but its influence on cirrus formation requires favourable temperature and ice-supersaturation conditions. Enhanced cirrus reflectance is therefore physically consistent with dust-related modification of ice-cloud formation. However, the weak and seasonally inconsistent response of effective ice particle radius does not provide sufficient evidence for a specific microphysical pathway, and heterogeneous ice nucleation should be regarded as a plausible interpretation rather than a directly demonstrated mechanism.

An important limitation is that Saharan dust transport and cloud formation are both closely linked to synoptic meteorological conditions. Moisture transport, vertical motion, temperature, and upper-tropospheric humidity may therefore contribute to the observed associations. Consequently, the results demonstrate a robust dust–cloud association, but do not establish causality. Long-term changes in the occurrence of conditions favourable for ice supersaturation could also contribute to a possible strengthening cirrus response, although such conditions were not directly quantified in this study.

4.3 Connection to increase of ice-supersaturated regions

Our results are consistent with recent studies reporting an increasing frequency of high relative humidity and ice-supersaturated conditions across the mid-latitudes of the Northern Hemisphere. Recent investigations suggest that the most pronounced change is not necessarily an increase in mean upper-tropospheric humidity, but rather a growing frequency of humidity conditions that are critical for cirrus formation (Benetatos et al., 2024). Because ice-supersaturated regions represent the primary thermodynamic environment for natural cirrus development, their increasing occurrence may provide increasingly favourable conditions for heterogeneous ice nucleation. Under such conditions, more frequent Saharan dust intrusions may increase the availability of mineral-dust INPs in atmospheric environments favourable for cirrus formation, although the present analysis does not directly quantify this mechanism (Varga et al., 2026; Weger et al., 2018).

The observed temporal evolution of dust-associated cirrus properties cannot be explained solely by changes in aerosol availability. It is likely also linked to ongoing modifications in the thermodynamic structure of the upper troposphere. Our previous studies have shown that the increasing frequency of Saharan dust intrusions reaching the Carpathian Basin may be related to the increasingly meridional and meandering character of the jet stream, which enhances the northward transport of dust-laden air masses from the Mediterranean and North Africa (Varga, 2020). The jet-stream environment is simultaneously recognized as one of the most important regions for ISSR formation, as frontal zones, upper-tropospheric divergence, and large-scale ascent associated with jet dynamics promote the development of ice-saturated and ice-supersaturated conditions (Hildebrandt et al., 2026; Spichtinger et al., 2005). Consequently, the jet stream and the mid-latitude storm tracks jointly regulate both upper-tropospheric moisture conditions and the thermodynamic prerequisites for cirrus formation. Eleftheratos et al. (2007) likewise demonstrated that cirrus cloud variability is closely linked to upper-tropospheric humidity and vertical motions, and that European cirrus variability is partly controlled by the North Atlantic Oscillation and associated circulation patterns. These common dynamical controls provide a physically plausible framework in which meridional circulation changes may simultaneously influence Saharan dust transport and the occurrence of upper-tropospheric conditions favourable for cirrus formation.

Recent studies investigating upper-tropospheric humidity (UTH) conditions suggest that the average moisture content of the upper troposphere does not necessarily exhibit a strong long-term increase (globally, ice-relative UTH has increased by approximately $+0.15\,\%$ per decade). Instead, the frequency of high relative humidity conditions with respect to ice, including saturated and supersaturated states, has increased more substantially, by approximately $+0.3\,\%$ to $+0.7\,\%$ per decade (Benetatos et al., 2024). This strengthening of the upper tail of the humidity distribution is particularly important for cirrus cloud formation, as these relatively short-lived but microphysically critical conditions promote ice nucleation and support the persistence of extensive cirrus cloud layers. Thus, it is primarily the frequency of ice-saturated and ice-supersaturated conditions, rather than mean upper-tropospheric humidity itself, that has increased during recent decades. Although climate models do not show a completely consistent signal regarding future ISSR occurrence over the Northern Hemisphere mid-latitudes (40–60° N), several studies suggest a modest increase. Benetatos et al. (2024) demonstrated that between 1979 and 2020 both upper-tropospheric humidity and the occurrence frequency of ice-saturated and supersaturated conditions increased over the mid-latitudes, with the latter exhibiting an even stronger trend. Particularly noteworthy is the finding that occurrences of high UTHi values ($> 70\,\%$, $> 80\,\%$, $> 90\,\%$, and $> 100\,\%$) increased significantly throughout the 30–60° N latitude belt, implying that environmental conditions favourable for cirrus formation have become progressively more common.

Regional European studies provide additional support for the mechanisms proposed here. Lidar observations from southern France (Hoareau et al., 2013) and Rome (Gobbi et al., 2004) demonstrate that cirrus clouds are frequent and climatologically important features of the European mid-latitude atmosphere. Cirrus occurrence frequencies of ap-

proximately 37 %–54 % were reported over southern France, while cirrus clouds were observed on nearly 45 % of measurement days over Rome. In both regions, maximum frequencies occurred during the spring and autumn transition seasons.

The Italian observations are particularly relevant in the context of aerosol–cirrus interactions. Over Rome, Saharan dust was present on approximately 20 % of observation days, primarily within the 2–6 km altitude range between boundary-layer aerosols and cirrus layers located between 6 and 14 km. These observations demonstrate the recurrent vertical proximity of Saharan dust layers and cirrus clouds over the Mediterranean region, although they do not by themselves establish a causal dust-induced ice-nucleation effect. Together, these studies indicate that cirrus cloud properties across the Mediterranean and southern Europe are influenced not only by meteorological conditions but also by long-range transported aerosols, particularly Saharan mineral dust, which regularly reaches the region and may provide effective INPs for upper-tropospheric cloud formation.

Direct observational evidence for this mechanism was provided by Ansmann et al. (2019) using combined lidar and radar measurements over Cyprus. The authors found a close correspondence between predicted INP concentrations and observed ice crystal concentrations within Saharan dust-containing middle- and upper-tropospheric cloud layers. The investigated cirrus clouds formed at altitudes between 8 and 11 km and temperatures ranging from −35 to −57 °C, and in several cases the observed ice crystal concentrations could be fully explained by the available dust-derived INPs. Particularly noteworthy is the "dust-infused baroclinic storm" (DIBS) case described by the authors, in which a North African dust outbreak injected large quantities of Saharan dust into the upper troposphere. The resulting dust-enriched cirrus system could be tracked for more than 3500 km from the Mediterranean to Central Asia, and the study concluded that mineral dust substantially contributed to the persistence and longevity of the cirrus cloud system. Similar dust-cirrus interactions were described in detail by other (Central) European studies (Seifert et al., 2023; Weger et al., 2018). These observations provide independent evidence that Saharan mineral dust can coexist with and contribute to ice formation at cirrus-relevant altitudes, thereby supporting the physical plausibility of the statistical associations identified in the present study.

4.4 Possible implications for mixed-phase cloud formation

Although the present study primarily focuses on cirrus clouds, the observed increase in mid-level cloud fraction with increasing atmospheric dust loading suggests that Saharan mineral dust may also influence cloud processes outside the classical cirrus regime. Mixed-phase clouds, containing both supercooled liquid droplets and ice crystals, frequently occur within the temperature range between approximately 0 and −38 °C and represent one of the largest remaining uncertainties in aerosol–cloud interactions and climate feedbacks (Storelvmo, 2017).

Mineral dust particles are known to be highly efficient INPs not only under cirrus-forming conditions but also within mixed-phase clouds (Atkinson et al., 2013; Hoose et al., 2008; Wiacek et al., 2010). Enhanced concentrations of dust-derived INPs may promote heterogeneous freezing of supercooled droplets, thereby accelerating glaciation processes and modifying cloud lifetime, cloud fraction, precipitation formation, and radiative properties. Depending on thermodynamic conditions, increased ice formation may either enhance precipitation and cloud dissipation through the Wegener–Bergeron–Findeisen process or increase cloud persistence through continuous ice crystal production.

The positive relationship observed between atmospheric dust loading and middle-level cloud fraction is therefore noteworthy. Previous studies have demonstrated the importance of Saharan dust for heterogeneous ice formation in European cloud systems (Seifert et al., 2010), while recent findings indicate that dust-driven droplet freezing can explain cloud-top phase in the northern extratropics (Villanueva et al., 2025). Although our datasets do not allow direct identification of mixed-phase cloud processes, these findings provide a physically plausible context for the observed dust-associated middle-cloud anomalies. Further investigations combining vertically resolved cloud-phase observations with thermodynamic profiles would be needed to quantify the contribution of mineral dust to these regional cloud changes.

4.5 Radiative implications

The radiative implications identified in this study are consistent with recent findings reported in the international literature. Cirrus clouds occupy a unique position within the Earth's radiation budget because, unlike most cloud types, they exhibit a relatively limited ability to reflect incoming shortwave radiation while efficiently absorbing and reemitting outgoing longwave radiation from the surface and lower troposphere. As a result, optically thin and moderately thick cirrus clouds generally exert a net warming effect, primarily manifested through a reduction in outgoing longwave radiation.

In a twenty-year lidar-based study conducted over Greenbelt, Maryland, Lolli et al. (2026) demonstrated that the radiative effects of cirrus clouds exhibit measurable long-term trends and that changes in cloud–radiation interactions play an important role in regional energy budgets. The authors emphasized that long-term monitoring of the optical and macrophysical properties of cirrus clouds is essential for understanding radiative processes associated with climate change.

Our findings can also be placed within a broader climatological context provided by recent satellite-based radia-

tion studies. Studies showed that the radiative characteristics of the Northern Hemisphere have undergone substantial changes during the past two decades, driven by combined variations in aerosols, atmospheric moisture, and cloud cover (Hodnebrog et al., 2024; Loeb et al., 2021). According to their results, cloud–radiation interactions represent one of the key contributors to the development of hemispheric radiative asymmetries. The observed dust-associated variations in cirrus reflectance, high-cloud fraction, and OLR may therefore be considered within this broader context of changing aerosol, cloud, and radiative conditions, although the present regional analysis does not establish a direct connection to hemispheric-scale radiative trends. Our results suggest that Saharan mineral dust at mid-latitudes may influence not only the microphysical properties of clouds but also contribute to upper-tropospheric energy exchange through the radiative effects associated with dust-related high-level ice clouds.

5 Conclusions

The aim of this study was to investigate the relationship between Saharan mineral dust and upper-level ice clouds over Hungary during the period 2001–2025. Using independent satellite and reanalysis datasets (MERRA-2, MODIS, and HIRS), we found a persistent but temporally evolving association between atmospheric dust loading and upper-level cloud properties, with the clearest long-term change occurring in the optical response of cirrus under high springtime dust loading.

The event-based analysis of 276 independently identified Saharan dust events provided further evidence for a systematic dust–cirrus association. SDEs were characterized by significantly enhanced cirrus reflectance and high-cloud fraction and by higher and colder cloud tops, with the most coherent response occurring in spring. These patterns were consistently supported by event–background comparisons, effect-size estimates, and direct comparisons between SDEs with lower and higher upper-tropospheric dust concentrations. The vertically resolved analysis showed that the strongest cloud anomalies occurred during SDEs with enhanced mineral dust concentrations at 7–12 km. Relative to low-dust reference conditions, high-Dust7–12 SDEs were characterized by substantially greater cirrus reflectance and high-cloud fraction and by higher and colder cloud tops in all seasons. The response was particularly coherent in spring, when cirrus reflectance and high-cloud fraction were 272 % and 133 % higher, respectively, while effective ice particle radius was 7.2 % smaller and OLR 14.4 % lower than under low-dust conditions. The direct comparison between SDE subsets further showed significantly smaller ice particle radii during high- than during low-Dust7–12 spring events.

The descriptive five-year springtime comparison suggested a more pronounced cirrus-reflectance enhancement during high-Dust7–12 SDEs in the later part of the study period. The relative difference from low-dust reference conditions increased from 143 % in 2001–2005 to 398 % in 2021–2025. However, this temporal pattern is based on period-specific median comparisons and does not establish a statistically significant long-term trend. Collectively, the results indicate increasingly frequent Saharan dust intrusions and a more pronounced springtime cirrus optical response during SDEs containing substantial dust at cirrus-relevant altitudes, rather than a uniform strengthening across all investigated cloud and radiative properties.

Our findings are consistent with previous studies identifying Saharan dust as an efficient source of INPs and with recent evidence for increasing ice-supersaturated conditions in the mid-latitude upper troposphere. However, this study advances current knowledge by showing that the dust–cirrus relationship has evolved over the past 25 years, with the clearest evidence of strengthening found in the cirrus optical response. This is consistent with the possibility that changes in the upper-tropospheric thermodynamic environment have modified the conditions under which mineral dust is associated with cirrus formation.

The study is based on satellite observations and reanalysis products and therefore infers physical mechanisms from robust statistical relationships rather than direct in situ observations. Although the agreement among multiple independent datasets increases confidence in the results, the relative contributions of dust mineralogy, transport pathways, upper-tropospheric humidity, and atmospheric circulation remain unresolved and should be addressed by future observational and modelling studies. The observed changes in dust–cirrus associations suggest that future changes in atmospheric circulation and upper-tropospheric moisture may modify the climatic influence of mineral dust through aerosol–cloud interactions. Better representation of these evolving processes in weather and climate models will therefore be essential for improving estimates of regional cloud feedbacks and radiative forcing.

Data availability. The satellite observations and reanalysis datasets used in this study are publicly available from their respective data providers. MERRA-2 hourly aerosol diagnostics, including dust column mass density, are available from NASA GES DISC (https://doi.org/10.5067/KLICLTZ8EM9D, GMAO, 2015a), while three-hourly, three-dimensional aerosol mixing ratios are available at https://doi.org/10.5067/LTVB4GPCOTK2 (GMAO, 2015b). MODIS Level-3 daily cloud products from Terra and Aqua are available at https://doi.org/10.5067/MODIS/MOD08_D3.061 (Platnick et al., 2017a) and https://doi.org/10.5067/MODIS/MYD08_D3.061 (Platnick et al., 2017b), respectively. The event-specific dataset, compiled through the identification of Saharan dust events and the integration of multiple atmospheric variables, is not currently deposited in a public repository because it is maintained as part of an ongoing research database. The processed data supporting the

findings of this study are available from the corresponding author upon reasonable request.

Author contributions. Conceptualization: GV, AG, ÁR, Methodology: GV, FG, AC, Investigation: GV, Visualization: FG, AC, ÁR, Writing – original draft: GV, Writing – review & editing: GV.

Competing interests. The contact author has declared that none of the authors has any competing interests.

Disclaimer. Publisher's note: Copernicus Publications remains neutral with regard to jurisdictional claims made in the text, published maps, institutional affiliations, or any other geographical representation in this paper. The authors bear the ultimate responsibility for providing appropriate place names. Views expressed in the text are those of the authors and do not necessarily reflect the views of the publisher.

Acknowledgements. The research was supported by the NRDI projects FK138692. This work has been implemented by the National Multidisciplinary Laboratory for Climate Change (RRF-2.3.1-21-2022-00014) project within the framework of Hungary's National Recovery and Resilience Plan supported by the Recovery and Resilience Facility of the European Union. The research was funded by the Sustainable Development and Technologies National Programme of the Hungarian Academy of Sciences (FFT NP FTA). This work was supported by the Ministry for Innovation and Technology of Hungary from the National Research, Development and Innovation Fund, financed under the 2021 Thematic Excellence Program funding scheme (grant number TKP2021-NKTA-21).

Financial support. This research has been supported by the Nemzeti Kutatási Fejlesztési és Innovációs Hivatal (grant nos. FK138692, RRF-2.3.1-21-2022-00014, and TKP2021-NKTA-21) and the Magyar Tudományos Akadémia (FFT NP FTA).

Review statement. This paper was edited by Martina Krämer and reviewed by Iarla Boyce and two anonymous referees.

References

Ansmann, A., Bösenberg, J., Chaikovsky, A., Comerón, A., Eckhardt, S., Eixmann, R., Freudenthaler, V., Ginoux, P., Komguem, L., Linné, H., Márquez, M. Á. L., Matthias, V., Mattis, I., Mitev, V., Müller, D., Music, S., Nickovic, S., Pelon, J., Sauvage, L., Sobolewsky, P., Srivastava, M. K., Stohl, A., Torres, O., Vaughan, G., Wandinger, U., and Wiegner, M.: Long-range transport of Saharan dust to northern Europe: The 11–16 October 2001 outbreak observed with EARLINET, J. Geophys. Res.-Atmos., 108, 4783, https://doi.org/10.1029/2003JD003757, 2003.

Ansmann, A., Mamouri, R.-E., Bühl, J., Seifert, P., Engelmann, R., Hofer, J., Nisantzi, A., Atkinson, J. D., Kanji, Z. A., Sierau, B., Vrekoussis, M., and Sciare, J.: Ice-nucleating particle versus ice crystal number concentrationin altocumulus and cirrus layers embedded in Saharan dust:a closure study, Atmos. Chem. Phys., 19, 15087–15115, https://doi.org/10.5194/acp-19-15087-2019, 2019.

Atkinson, J. D., Murray, B. J., Woodhouse, M. T., Whale, T. F., Baustian, K. J., Carslaw, K. S., Dobbie, S., O'Sullivan, D., and Malkin, T. L.: The importance of feldspar for ice nucleation by mineral dust in mixed-phase clouds, Nature, 498, 355–358, https://doi.org/10.1038/nature12278, 2013.

Benetatos, C., Eleftheratos, K., Gierens, K., and Zerefos, C.: A statistically significant increase in ice supersaturation in the atmosphere in the past 40 years, Sci. Rep., 14, 24760, https://doi.org/10.1038/s41598-024-75756-9, 2024.

Benjamini, Y. and Hochberg, Y.: Controlling the False Discovery Rate: A Practical and Powerful Approach to Multiple Testing, J. R. Stat. Soc. B, 57, 289–300, https://doi.org/10.1111/j.2517-6161.1995.tb02031.x, 1995.

Boucher, O., Randall, D., Artaxo, P., Bretherton, C., Feingold, G., Forster, P., Kerminen, V.-M., Kondo, Y., Liao, H., and Lohmann, U.: Clouds and aerosols, in: Climate change 2013: The physical science basis. Contribution of working group I to the fifth assessment report of the intergovernmental panel on climate change, Cambridge University Press, 571–657, https://doi.org/10.1017/CBO9781107415324.016, 2013.

Chatziparaschos, M., Daskalakis, N., Myriokefalitakis, S., Kalivitis, N., Nenes, A., Gonçalves Ageitos, M., Costa-Surós, M., Pérez García-Pando, C., Zanoli, M., Vrekoussis, M., and Kanakidou, M.: Role of K-feldspar and quartz in global ice nucleation by mineral dust in mixed-phase clouds, Atmos. Chem. Phys., 23, 1785–1801, https://doi.org/10.5194/acp-23-1785-2023, 2023.

Cuevas-Agulló, E., Barriopedro, D., García, R. D., Alonso-Pérez, S., González-Alemán, J. J., Werner, E., Suárez, D., Bustos, J. J., García-Castrillo, G., García, O., Barreto, Á., and Basart, S.: Sharp increase in Saharan dust intrusions over the western Euro-Mediterranean in February–March 2020–2022 and associated atmospheric circulation, Atmos. Chem. Phys., 24, 4083–4104, https://doi.org/10.5194/acp-24-4083-2024, 2024.

DeMott, P., Sassen, K., Poellot, M., Baumgardner, D., Rogers, D., Brooks, S., Prenni, A., and Kreidenweis, S.: African dust aerosols as atmospheric ice nuclei, Geophys. Res. Lett., 30, https://doi.org/10.1029/2003GL017410, 2003.

DeMott, P. J., Prenni, A. J., Liu, X., Kreidenweis, S. M., Petters, M. D., Twohy, C. H., Richardson, M. S., Eidhammer, T., and Rogers, D. C.: Predicting global atmospheric ice nuclei distributions and their impacts on climate, P. Natl. Acad. Sci. USA, 107, 11217–11222, https://doi.org/10.1073/pnas.0910818107, 2010.

Eleftheratos, K., Zerefos, C. S., Zanis, P., Balis, D. S., Tselioudis, G., Gierens, K., and Sausen, R.: A study on natural and man-made global interannual fluctuations of cirrus cloud cover for the period 1984–2004, Atmos. Chem. Phys., 7, 2631–2642, https://doi.org/10.5194/acp-7-2631-2007, 2007.

Global Modeling and Assimilation Office (GMAO): MERRA-2 tavg1_2d_aer_Nx: 2d, 1-Hourly, Time-Averaged, Single-Level, Assimilation, Aerosol Diagnostics, V5.12.4, NASA GES DISC [data set], https://doi.org/10.5067/KLICLTZ8EM9D, 2015a.

Global Modeling and Assimilation Office (GMAO): MERRA-2 inst3_3d_aer_Nv: 3d, 3-Hourly, Instantaneous, Model-Level, Assimilation, Aerosol Mixing Ratio, V5.12.4, NASA GES DISC [data set], https://doi.org/10.5067/LTVB4GPCOTK2, 2015b.

Gobbi, G. P., Barnaba, F., and Ammannato, L.: The vertical distribution of aerosols, Saharan dust and cirrus clouds in Rome (Italy) in the year 2001, Atmos. Chem. Phys., 4, 351–359, https://doi.org/10.5194/acp-4-351-2004, 2004.

Harrison, A. D., Lever, K., Sanchez-Marroquin, A., Holden, M. A., Whale, T. F., Tarn, M. D., McQuaid, J. B., and Murray, B. J.: The ice-nucleating ability of quartz immersed in water and its atmospheric importance compared to K-feldspar, Atmos. Chem. Phys., 19, 11343–11361, https://doi.org/10.5194/acp-19-11343-2019, 2019.

Heymsfield, A. J., Krämer, M., Brown, P., Cziczo, D. J., Franklin, C., Lawson, R. P., Lohmann, U., Luebke, A., McFarquhar, G. M., Ulanowski, Z., and Van Tricht, K.: Cirrus Clouds, Meteor. Mon., 58, 2.1–2.26, https://doi.org/10.1175/AMSMONOGRAPHS-D-16-0010.1, 2017.

Hildebrandt, K. G., Castino, F., Meijer, V., and Yin, F.: Variability of ice supersaturated regions at flight altitudes: evaluation of ERA5 reanalysis using IAGOS in situ measurements, Atmos. Chem. Phys., 26, 6449–6470, https://doi.org/10.5194/acp-26-6449-2026, 2026.

Hoareau, C., Keckhut, P., Noel, V., Chepfer, H., and Baray, J.-L.: A decadal cirrus clouds climatology from ground-based and spaceborne lidars above the south of France (43.9° N–5.7° E), Atmos. Chem. Phys., 13, 6951–6963, https://doi.org/10.5194/acp-13-6951-2013, 2013.

Hodnebrog, Ø., Myhre, G., Jouan, C., Andrews, T., Forster, P. M., Jia, H., Loeb, N. G., Olivié, D. J. L., Paynter, D., Quaas, J., Raghuraman, S. P., and Schulz, M.: Recent reductions in aerosol emissions have increased Earth's energy imbalance, Commun. Earth Environ., 5, 166, https://doi.org/10.1038/s43247-024-01324-8, 2024.

Hoose, C. and Möhler, O.: Heterogeneous ice nucleation on atmospheric aerosols: a review of results from laboratory experiments, Atmos. Chem. Phys., 12, 9817–9854, https://doi.org/10.5194/acp-12-9817-2012, 2012.

Hoose, C., Lohmann, U., Erdin, R., and Tegen, I.: The global influence of dust mineralogical composition on heterogeneous ice nucleation in mixed-phase clouds, Environ. Res. Lett., 3, 025003, https://doi.org/10.1088/1748-9326/3/2/025003, 2008.

Irvine, E. A. and Shine, K. P.: Ice supersaturation and the potential for contrail formation in a changing climate, Earth Syst. Dynam., 6, 555–568, https://doi.org/10.5194/esd-6-555-2015, 2015.

Juurikkala, K., Raatikainen, T., Krämer, M., Williamson, C. J., and Laaksonen, A.: Mineral dust concentration controlling convective cirrus structure and persistence: a large-eddy simulation study with observational constraints, Atmos. Chem. Phys., 26, 16173–16202, https://doi.org/10.5194/acp-26-16173-2026, 2026.

Kanji, Z. A., Ladino, L. A., Wex, H., Boose, Y., Burkert-Kohn, M., Cziczo, D. J., and Krämer, M.: Overview of Ice Nucleating Particles, Meteorol. Mon., 58, 1.1–1.33, https://doi.org/10.1175/AMSMONOGRAPHS-D-16-0006.1, 2017.

Kärcher, B.: Formation and radiative forcing of contrail cirrus, Nat. Commun., 9, 1824, https://doi.org/10.1038/s41467-018-04068-0, 2018.

Kärcher, B., DeMott, P. J., Jensen, E. J., and Harrington, J. Y.: Studies on the Competition Between Homogeneous and Heterogeneous Ice Nucleation in Cirrus Formation, J. Geophys. Res.-Atmos., 127, https://doi.org/10.1029/2021JD035805, 2022.

Kärcher, B., Jensen, E. J., Pokrifka, G. F., and Harrington, J. Y.: Ice Supersaturation Variability in Cirrus Clouds: Role of Vertical Wind Speeds and Deposition Coefficients, J. Geophys. Res.-Atmos., 128, https://doi.org/10.1029/2023JD039324, 2023.

Knopf, D. A. and Alpert, P. A.: Atmospheric ice nucleation, Nat. Rev. Phys., 5, 203–217, https://doi.org/10.1038/s42254-023-00570-7, 2023.

Kok, J. F., Storelvmo, T., Karydis, V. A., Adebiyi, A. A., Mahowald, N. M., Evan, A. T., He, C., and Leung, D. M.: Mineral dust aerosol impacts on global climate and climate change, Nat. Rev. Earth Environ., 4, 71–86, https://doi.org/10.1038/s43017-022-00379-5, 2023.

Krämer, M., Rolf, C., Luebke, A., Afchine, A., Spelten, N., Costa, A., Meyer, J., Zöger, M., Smith, J., Herman, R. L., Buchholz, B., Ebert, V., Baumgardner, D., Borrmann, S., Klingebiel, M., and Avallone, L.: A microphysics guide to cirrus clouds – Part 1: Cirrus types, Atmos. Chem. Phys., 16, 3463–3483, https://doi.org/10.5194/acp-16-3463-2016, 2016.

Krämer, M., Rolf, C., Spelten, N., Afchine, A., Fahey, D., Jensen, E., Khaykin, S., Kuhn, T., Lawson, P., Lykov, A., Pan, L. L., Riese, M., Rollins, A., Stroh, F., Thornberry, T., Wolf, V., Woods, S., Spichtinger, P., Quaas, J., and Sourdeval, O.: A microphysics guide to cirrus – Part 2: Climatologies of clouds and humidity from observations, Atmos. Chem. Phys., 20, 12569–12608, https://doi.org/10.5194/acp-20-12569-2020, 2020.

Krämer, M., Spelten, N., Rolf, C., and Spang, R.: A microphysics guide to cirrus – Part 3: Occurrence patterns of cloud particles, Atmos. Chem. Phys., 25, 13563–13583, https://doi.org/10.5194/acp-25-13563-2025, 2025.

Liou, K.-N.: Influence of Cirrus Clouds on Weather and Climate Processes: A Global Perspective, Mon. Weather Rev., 114, 1167–1199, https://doi.org/10.1175/1520-0493(1986)114<1167:IOCCOW>2.0.CO;2, 1986.

Loeb, N. G., Johnson, G. C., Thorsen, T. J., Lyman, J. M., Rose, F. G., and Kato, S.: Satellite and Ocean Data Reveal Marked Increase in Earth's Heating Rate, Geophys. Res. Lett., 48, e2021GL093047, https://doi.org/10.1029/2021GL093047, 2021.

Lolli, S., Dolinar, E. K., Lewis, J. R., Salcedo-Bosch, A., Campbell, J. R., and Welton, E. J.: Long-term trends in daytime cirrus cloud radiative effects: analyzing twenty years of Micropulse Lidar Network measurements at Greenbelt, Maryland in eastern North America, Atmos. Chem. Phys., 26, 411–426, https://doi.org/10.5194/acp-26-411-2026, 2026.

Mann, H. B. and Whitney, D. R.: On a Test of Whether one of Two Random Variables is Stochastically Larger than the Other, Ann. Math. Stat., 18, 50–60, https://doi.org/10.1214/aoms/1177730491, 1947.

Niemand, M., Möhler, O., Vogel, B., and Vogel, H.: A Particle-Surface-Area-Based Parameterization of Immersion Freezing on Desert Dust Particles, J. Atmos. Sci., 69, 3077–3092, https://doi.org/10.1175/JAS-D-11-0249.1, 2012.

Pey, J., Querol, X., Alastuey, A., Forastiere, F., and Stafoggia, M.: African dust outbreaks over the Mediterranean Basin during 2001–2011: PM_{10} concentrations, phenomenology and trends, and its relation with synoptic and mesoscale meteorology, Atmos. Chem. Phys., 13, 1395–1410, https://doi.org/10.5194/acp-13-1395-2013, 2013.

Pieper, L., Seifert, P., Griesche, H., Ansmann, A., McCosh, G., Ewald, F., and Kneifel, S.: Turbulence structure of dusty cirrus and its relation to atmospheric conditions: A characterization using cloud-radar measurements and reanalysis data, EGUsphere [preprint], https://doi.org/10.5194/egusphere-2026-3092, 2026.

Platnick, S., King, M., and Hubanks, P.: MODIS/Terra Atmosphere L3 Daily Global Product, Collection 6.1, NASA MODIS Adaptive Processing System, Goddard Space Flight Center [data set], https://doi.org/10.5067/MODIS/MOD08_D3.061, 2017a.

Platnick, S., King, M., and Hubanks, P.: MODIS/Aqua Atmosphere L3 Daily Global Product, Collection 6.1, NASA MODIS Adaptive Processing System, Goddard Space Flight Center [data set], https://doi.org/10.5067/MODIS/MYD08_D3.061, 2017b.

Rodríguez, S. and López-Darias, J.: Extreme Saharan dust events expand northward over the Atlantic and Europe, prompting record-breaking PM_{10} and $PM_{2.5}$ episodes, Atmos. Chem. Phys., 24, 12031–12053, https://doi.org/10.5194/acp-24-12031-2024, 2024.

Rogora, M., Mosello, R., and Marchetto, A.: Long-term trends in the chemistry of atmospheric deposition in Northwestern Italy: the role of increasing Saharan dust deposition, Tellus B, 56, 426–434, https://doi.org/10.3402/tellusb.v56i5.16456, 2004.

Salvador, P., Pey, J., Pérez, N., Querol, X., and Artíñano, B.: Increasing atmospheric dust transport towards the western Mediterranean over 1948–2020, NPJ Clim. Atmos. Sci., 5, 34, https://doi.org/10.1038/s41612-022-00256-4, 2022.

Seifert, A., Bachmann, V., Filipitsch, F., Förstner, J., Grams, C. M., Hoshyaripour, G. A., Quinting, J., Rohde, A., Vogel, H., Wagner, A., and Vogel, B.: Aerosol–cloud–radiation interaction during Saharan dust episodes: the dusty cirrus puzzle, Atmos. Chem. Phys., 23, 6409–6430, https://doi.org/10.5194/acp-23-6409-2023, 2023.

Seifert, P., Ansmann, A., Mattis, I., Wandinger, U., Tesche, M., Engelmann, R., Müller, D., García-Pando, C. P., and Haustein, K.: Saharan dust and heterogeneous ice formation: Eleven years of cloud observations at a central European EARLINET site, J. Geophys. Res., 115 https://doi.org/10.1029/2009JD013222, 2010.

Spichtinger, P., Gierens, K., and Dörnbrack, A.: Formation of ice supersaturation by mesoscale gravity waves, Atmos. Chem. Phys., 5, 1243–1255, https://doi.org/10.5194/acp-5-1243-2005, 2005.

Stein, A. F., Draxler, R. R., Rolph, G. D., Stunder, B. J. B., Cohen, M. D., and Ngan, F.: NOAA's HYSPLIT Atmospheric Transport and Dispersion Modeling System, B. Am. Meteorol. Soc., 96, 2059–2077, https://doi.org/10.1175/BAMS-D-14-00110.1, 2015.

Storelvmo, T.: Aerosol Effects on Climate via Mixed-Phase and Ice Clouds, Annu. Rev. Earth Pl. Sc., 45, 199–222, https://doi.org/10.1146/annurev-earth-060115-012240, 2017.

Twomey, S.: Pollution and the planetary albedo, Atmos. Environ., 8, 1251–1256, https://doi.org/10.1016/0004-6981(74)90004-3, 1974.

Ullrich, R.: A New Ice Nucleation Active Site Parameterization for Desert Dust and Soot, J. Atmos. Sci., 74, 699–717, https://doi.org/10.1175/JAS-D-16-0074.1, 2017.

Varga, G.: Changing nature of Saharan dust deposition in the Carpathian Basin (Central Europe): 40 years of identified North African dust events (1979–2018), Environ. Int., 139, 105712, https://doi.org/10.1016/j.envint.2020.105712, 2020.

Varga, G., Kovács, J., and Újvári, G.: Analysis of Saharan dust intrusions into the Carpathian Basin (Central Europe) over the period of 1979–2011, Global Planet. Change, 100, 333–342, https://doi.org/10.1016/j.gloplacha.2012.11.007, 2013.

Varga, G., Gresina, F., Gelencsér, A., Csávics, A., and Rostási, Á.: Saharan dust and cirrus clouds: Dominating indirect impact of dust events on photovoltaic energy generation in Hungary (2019–2024), Sol. Energy, 307, 114385, https://doi.org/10.1016/j.solener.2026.114385, 2026.

Villanueva, D., Stengel, M., Hoose, C., Bruno, O., Jeggle, K., Ansmann, A., and Lohmann, U.: Dust-driven droplet freezing explains cloud-top phase in the northern extratropics, Science, 389, 521–525, https://doi.org/10.1126/science.adt5354, 2025.

Weger, M., Heinold, B., Engler, C., Schumann, U., Seifert, A., Fößig, R., Voigt, C., Baars, H., Blahak, U., Borrmann, S., Hoose, C., Kaufmann, S., Krämer, M., Seifert, P., Senf, F., Schneider, J., and Tegen, I.: The impact of mineral dust on cloud formation during the Saharan dust event in April 2014 over Europe, Atmos. Chem. Phys., 18, 17545–17572, https://doi.org/10.5194/acp-18-17545-2018, 2018.

Wiacek, A., Peter, T., and Lohmann, U.: The potential influence of Asian and African mineral dust on ice, mixed-phase and liquid water clouds, Atmos. Chem. Phys., 10, 8649–8667, https://doi.org/10.5194/acp-10-8649-2010, 2010.